2018 IEEE Conference on Decision and Control (CDC)
Miami Beach, FL, USA, Dec. 17-19, 2018

A velocity observer for exterior ballistics using an embedded frequency detection of pitch and yaw aerodynamics

Aurélien Fiot[1] Sébastien Changey[2] Christophe Combettes[2] Nicolas Petit[3]

***Abstract*— This article proposes a methodology for estimating the velocity (w.r.t the air) of a high-velocity flying shell from low-cost embedded sensors. The novelty is to exploit aerodynamics models in combination with a frequency detection approach, through a state observer. Besides its main rotation (spin), the shell has gyroscopic precession and nutation motions, which are measured by inertial sensors as pseudo-periodic signals. The instantaneous frequencies of these time-varying signals give direct information on the aerodynamics of the shell, and in particular, its velocity w.r.t the air. The frequency content of the signal of the strapdown sensors is exploited by means of a two-step approach consisting of frequency detection reconciled with the aerodynamic models by an observer. A switching gain is used to deal with the transition of the shell in the transonic regime. A proof of convergence is given. Experimental results are exposed.**

I. INTRODUCTION

This article exposes a methodology for estimating the velocity w.r.t the air of a high-velocity flying shell. The problem under consideration belongs to the vast class of state estimation problem for 6-degrees of freedom (DOF) rigid bodies subjected to aerodynamics effects using embedded sensors. As it is now very common with the advent of low-cost sensors, such solid body can be equipped with strapdown inertial sensors, which as is well known [1], [2], [3], [4], [5], [6], [7], [8], [9], [10], [11], [12] can be used to reliably solve navigation problems, at the expense of reasonably complex on-board calculations and off-line tasks such as multi-sensor system calibration [13]. Numerous experiments have been reported in the literature for Unmanned aerial vehicles [14], [15], [16], Unmanned ground vehicles [17], micro-satellites [18], [19], [20], sounding rockets [21], space-crafts [22], [23], [24] among others.

However, in some applications, such as the artillery shells which are the example we focus on in this study, several constraints discard these classic techniques. Lately, this topic has been of interest as significant performance improvements are expected from "smart-shells" (compared to currently employed ammunitions) which embed sensors for guidance and navigation tasks [25], [26], [27]. The trajectory of a shell is short due to its high speed, and can be subjected to a high spinning rate [28], [29], [30]. The short duration of the flight is unfavourable to GPS sensors, which usually work at low measurement rates. On the other hand, the spin can saturate most low-cost gyrometers[1], if they are not damaged by the high impact caused by the gunshot. These facts make the navigation problem a difficult one.

In this article, we propose an unusual method to solve one central question in navigation of shells: the estimation of its velocity w.r.t. the air, as already considered in [31], [32], [33]. The novel method we propose takes advantage of the oscillations the shell is subjected to. The pendulum-like rotation dynamics is created by aerodynamics effects in a way that is well understood and documented [28]. Our idea is to detect the instantaneous frequencies of the yawing and pitching oscillations and to interpret them as information on the velocity. In details, we estimate one or several frequencies using a super-resolution technique and deduce the value of the velocity from a state observer filtering this information and reconciling it with *a priori* knowledge taking the form of analytic expressions involving aerodynamic look-up tables available for the specific shell under consideration. The technique employs frequency detection algorithms ([34]) that are well suited for the time-varying signals generated during the ballistic flight. The paper presents the whole methodology, initiated in [35], starting from a frequency analysis of the equations of motion, exposing the observer design along with a proof of convergence, and reporting experimental results.

II. PROBLEM STATEMENT

Notations

The main notations used in the aerodynamic model of the shell are listed in Table I. Each aerodynamic coefficient $\hat{C}_{\cdot}$ in this table is specific to the shell shape and size, and is a function of the Mach number and the incidence angles of the shell.

For application on gun launched (artillery) ammunition, a navigation system must satisfy various requirements : surviving the (strong) gun acceleration, enduring very high spinning rates, relying on low cost-sensors, being started in-flight. For these reasons, various research have considered algorithms using only accelerometers and magnetometers (leaving gyrometers out of the scope). Advantageously, some accurate aerodynamic models of the shell can be incorporated in the navigation algorithms *if an in-flight estimate of the Mach number is available*. For this reason the work presented in this article is of practical interest. In Figure 1, the typical structure of a navigation algorithm is described. The velocity information is instrumental to estimate the incidence of the shell.

The shells, in addition to being spin-stabilized to mitigate the effects of side wind, follow a gyroscopic precession and nutation motion (depicted by Figure 2). Those frequencies of the yawing and pitching motions can be observed on the raw measurements of the strapdown inertial sensors (although

[1]Aurélien Fiot is a PhD candidate at CAS - Centre automatique et systèmes, MINES ParisTech, PSL Research University, and the Guidance, Navigation and Control department at ISL

[2]Sébastien Changey and Christophe Combettes are Dr. Eng. in the Guidance, Navigation and Control department at ISL

[3]Nicolas Petit is Professor, CAS - Centre automatique et systèmes, MINES ParisTech, PSL Research University

[1]typically, rotation rates of 300 Hz can be considered, which is out of the scale of most low-cost gyrometers

M	Mass of the shell
D	Caliber of the shell
S	Section of the shell
I_l	Longitudinal moment of inertia
I_t	Transverse moment of inertia
v	Scalar velocity of the shell w.r.t the air
h	Altitude of the shell
$\rho_a(h)$	Air density
p	Spinning rate of the shell in the body frame
ω_p	Precession frequency of the shell
ω_n	Nutation frequency of the shell
$\hat{C}_D$	Drag force coefficient
$\hat{C}_{L\alpha}$	Lift force coefficient
$\hat{C}_{mag-f}$	Magnus force coefficient
$\hat{C}_{mag-m}$	Magnus moment coefficient
$\hat{C}_{l\delta}$	Rolling moment coefficient
$\hat{C}_{spin}$	Roll damping moment coefficient
$\hat{C}_{Mq}$	Pitch damping moment coefficient
$\hat{C}_{M\alpha}$	Overturning moment coefficient

TABLE I
NOMENCLATURE.

one needs to discriminate them from the spinning rate beforehand) and provide information on the aerodynamics of the shell. As it will be explained in Section 3, those frequencies carry information on the Mach number, the spinning rate of the shell and its aerodynamics coefficients. In this article, we propose a methodology to estimate this variable, which is pictured in Figure 3. It combines a frequency detection algorithm and a state observer.

III. FREQUENCY CONTENT OF THE EMBEDDED INERTIAL MEASURMENTS

The high velocity shell under consideration is a 6 DOF rigid body which is given a high initial translational velocity and a high spinning rate by the gun launch. The orientation of the rigid body is defined by a set of three Euler angles (here 'ZXZ' angles are chosen, following the nomenclature of [36], where, classically, the spin is defined as the rotation about its axis of least inertia). The shell is symmetrical and has a constant mass during the whole flight. It is subjected to drag and lift forces, Magnus, overturning, pitch-Damping and roll-damping moments [28], [37]. These forces and moments have been well-studied. Experimentally validated models are known (see e.g. [38], [39]). Compact expressions are given in Table II, they involve numerous lookup tables that will be discussed later on.

During the whole flight (typically lasting less than 45 sec for ballistic flight and less than 2 sec for flat-fire) the spinning

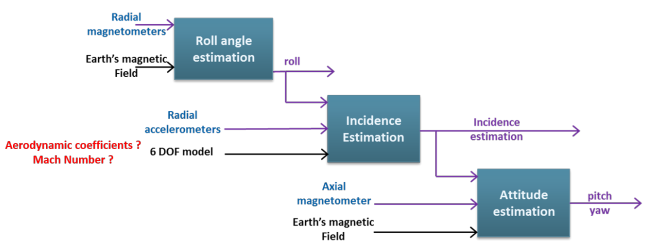

Fig. 1. Cascade filtering of a shell attitude and position. The velocity information is of interest to estimate the incidence of the shell.

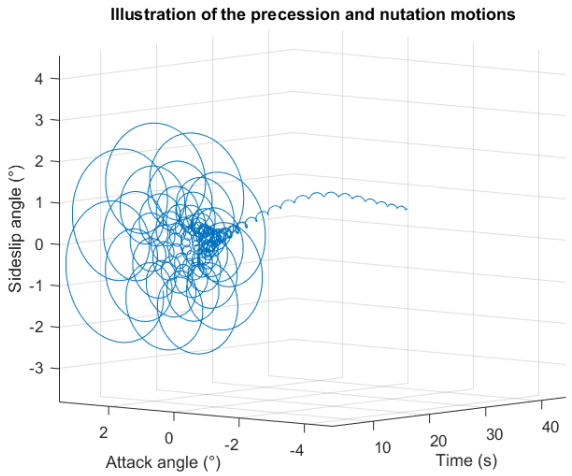

Fig. 2. Precession and nutation angles of the shell during a typical shell flight.

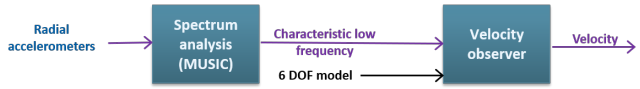

Fig. 3. Method to estimate the velocity of the shell.

Forces/Moments	Aerodynamic coefficients	Expression
Gravity force		$M\mathbf{g}$
Drag force	$\hat{C}_D$	$-\frac{1}{2}\rho S\hat{C}_D V\mathbf{v}_B^A$
Lift force	$\hat{C}_{L\alpha}$	$\frac{1}{2}\rho S\hat{C}_{L\alpha}(\mathbf{v}_B^A \wedge (\mathbf{b_1} \wedge \mathbf{v}_B^A))$
Magnus force	$\hat{C}_{mag\text{-}f}$	$\frac{1}{2}\rho S\left(\frac{pD}{V}\right)\hat{C}_{mag-f}V(\mathbf{v}_B^A \wedge \mathbf{b_1})$
Coriolis force		$2M\mathbf{v}_B^I \wedge \omega_L^I$
Magnus moment	$\hat{C}_{mag\text{-}m}$	$\frac{1}{2}\rho SD\left(\frac{pD}{V}\right)\hat{C}_{mag-m}V(\mathbf{b_1} \wedge (\mathbf{v}_B^A \wedge \mathbf{b_1}))$
Overturning moment	$\hat{C}_{M\alpha}$	$\frac{1}{2}\rho SD\hat{C}_{M\alpha}V(\mathbf{v}_B^A \wedge \mathbf{b_1})$
Rolling moment	$\hat{C}_{l\delta}$	$\frac{1}{2}\rho SD\delta_{fin\ cant}\hat{C}_{l\delta}V^2\mathbf{b_1}$
Pitch-damping moment	$\hat{C}_{Mq}$	$\frac{1}{2}\rho SD^2\hat{C}_{Mq}V(\mathbf{b_1} \wedge (\omega_B^I \wedge \mathbf{b_1}))$
Roll-damping moment	$\hat{C}_{spin}$	$\frac{1}{2}\rho SD\left(\frac{pD}{V}\right)\hat{C}_{spin}V^2\mathbf{b_1}$

TABLE II
LIST OF FORCES AND MOMENTS ACTING ON THE SHELL WITH COMPACT EXPRESSIONS FROM [28].

rate remains very high, and the angles of attitude w.r.t. the wind frame remain small. Therefore, it is possible to study the attitude dynamics, and the translational dynamics in turn, under the assumption of small-angles. Some lengthy calculations allow one to determine the frequencies appearing in the solution of these dynamics. These frequencies are the results of the interferences caused by the nutation, precession and spin rotations, and mirror the fast and slow epicyclic yaw mode described in [28].

Through these assumptions, the nutation and precession frequencies, ω_n and $\omega_p < \omega_n$ respectively, have the symmetrical forms (refer to Table I for notations)

$$\omega_n = \frac{pI_l}{2I_t} + \frac{v}{2D}(P_1^2 + P_2^2)^{\frac{1}{4}} \cos\left[\frac{1}{2}\arctan\left(\frac{P_2}{P_1}\right)\right] \quad (1)$$

$$\omega_p = \frac{pI_l}{2I_t} - \frac{v}{2D}(P_1^2 + P_2^2)^{\frac{1}{4}} \cos\left[\frac{1}{2}\arctan\left(\frac{P_2}{P_1}\right)\right] \quad (2)$$

where I_l and I_t are longitudinal and transverse inertial coefficients and where

$$P_1(v,h,p) = a_1(v,h)^2 - b_1(v,p)^2 - 4a_2(v,h)$$
$$P_2(v,h,p) = 4b_2(v,h,p) - 2a_1(v,h)b_1(v,h)$$

with

$$a_1(v,h) = -B_M\hat{C}_{mq} + B_F(\hat{C}_{L\alpha} - \hat{C}_D)$$
$$a_2(v,h) = -B_M\hat{C}_{M\alpha}$$
$$b_1(v,p) = \frac{p}{v}D\frac{I_l}{I_t}$$
$$b_2(v,h,p) = b_1(B_F\hat{C}_{L\alpha} - B_M\hat{C}_{mag-m}\frac{I_t}{I_l})$$
$$B_F(h) = \frac{\rho_a(h)SD}{2m}, \qquad B_M(h) = \frac{\rho_a(h)SD^3}{2I_t}$$

Aerodynamic drag near Mach 1.0

The aerodynamics coefficients appearing in these last factors are defined in Table II. Importantly, these aerodynamic coefficients are functions of the Mach number and are specific to the shell considered. $\hat{C}_D$ describes the drag force, $\hat{C}_{L\alpha}$ the lift force, $\hat{C}_{mag-m}$ the Magnus moment, $\hat{C}_{M\alpha}$ the overturning moment, and $\hat{C}_{mq}$ the pitch-damping moment. The Mach number is a function of the velocity and the altitude, as it depends on the air density surrounding the shell.

The drag is a dominant effect and deserves some more discussion. Some effects of the shell shape on the drag coefficient at various Mach numbers have long been studied [28]. Those effects depend on a number of dimensionless variables. The fluid mechanism that transmits the drag force to the shell consists of two parts: surface pressure and surface shear stress (a.k.a. skin friction drag). The force generated on the forebody and the base of the shell are different. Therefore, the various components of the drag force behave in significantly different ways in the various speed regions.

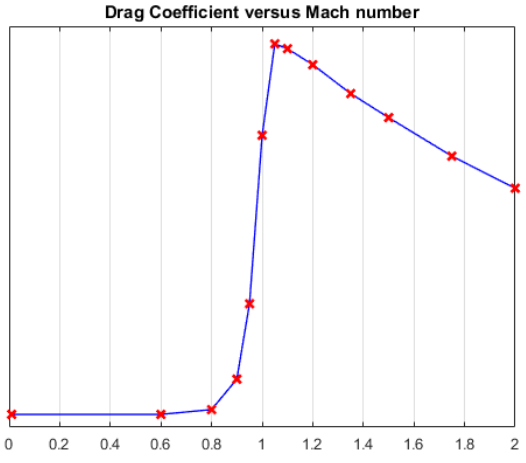

Fig. 4. Mapping of the considered drag coefficient (scales are omitted due to confidentiality reasons)

At subsonic flight speeds (below Mach 1.0), the drag coefficient is essentially constant. It rises sharply near Mach 1.0, then slowly decrease at higher supersonic speeds. The sudden rise appearing just below Mach 1.0 is caused by the formation of shock waves in the flow-field surrounding the shell [28].

IV. DYNAMIC FREQUENCY MEASUREMENT : MEASURING VARYING FREQUENCIES

A. Definition of the frequency of interest

The radial strapdown accelerometers measure a projection of the aerodynamic forces in the body frame. In other words, their signal is proportional to the incidence angles of the shell, containing the precession and nutation frequencies defined in eqs. (1) and (2).

In eqs. (1) and (2), the spinning rate p plays the same biasing role by a factor that is independent from the velocity. There are a number of possible choices to isolate the velocity-dependent factor appearing in both equations. Because p is easy to estimate (see e.g. [40], [41], [42], [43], [44], mostly because it is much higher than the nutation and precession rate), a simple strategy is to simply subtract it from the detected frequencies. In the following, we define our "measurement" ω_{meas} as

$$\omega_{\text{meas}} = \omega_n - \frac{p}{2}\frac{I_l}{I_t} = \frac{p}{2}\frac{I_l}{I_t} - \omega_p = \frac{\omega_n - \omega_p}{2} \tag{3}$$

This last equation stresses that the variable of interest ω_{meas} can be determined by three formulas, each of which have pros and cons, as will be briefly discussed in the numerical experiments in Section VI.

B. Frequency detection using super-resolution

A common practice to estimate the frequency of a monochromatic signal or a multisinusoidal signal is to use Fast Fourier Transform (FFT) over sliding windows. This state-of-the-art technique is at the heart of the periodogram technique [45] and is often employed in various applicative situations. It is not really well-suited in the case considered here. The main culprit is that FFT is only effective in cases where a relatively large window can be used to estimate the frequency. If this assumption fails, then numerous malicious effects appear such as spectral aliasing, and frequency leak [45]. This is not the case in the application considered here, because the signal from which frequency must be detected is decaying over time (see [35]). Employing a large window violates the assumption that the signal has constant magnitude, which is implicitly required for the FFT technique to produce quality results.

Instead, we use a super-resolution technique. In a nutshell, this technique is optimization-based (in the time domain). It seeks the frequencies of a multisinusoidal signal as the solution of a best-fit problem. Various implementations exist, from the classic Prony based methods (MUSIC [46]) to more recent total-variation norm minimization methods [34], [47]. On top of improving resolution, the methods have proven capabilities of outlier rejection even with high noise/signal ratios. To work effectively, super-resolution methods require that the numbers of frequencies to be located in the signal be known in advance. This is precisely the case in our application, as we have seen in it Section III. Super-resolution methods can deal with short time windows, typically half a period of the lowest frequency to be detected is enough. This is a very helpful feature in our case. We report in Figure 5,

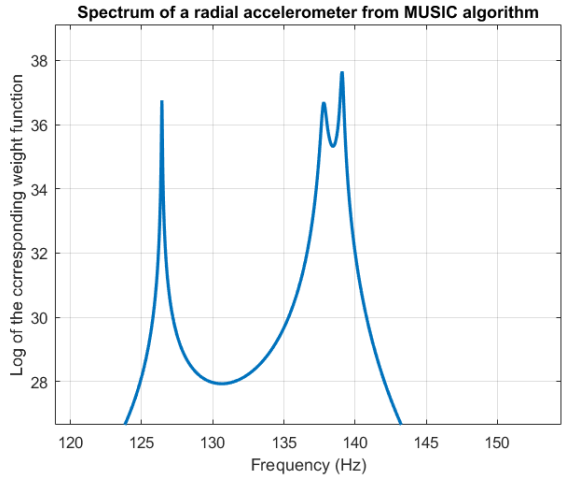

Fig. 5. Detection of the frequencies $p - \omega_n < p - \omega_p < p$ contained in the signal from one of the transverse accelerometers (simulation results).

a typical example where the spin, and linear combinations with nutation and precession frequencies are detected as the sharp peaks of the spectrum obtained from MUSIC.

Assuming that the frequency-detection algorithm discussed above has been implemented, we will now refer to its output as a measurement

$$y \triangleq \omega_{\text{meas}} \tag{4}$$

Even with relatively large amounts of noise, this output is relatively reliable. It is not noise-free, as the output of the super-resolution algorithm is by definition lying on a (fine) grid of possible values. On occasions, the algorithm may fail to provide a frequency value. Then, the measurement will be faulty. In all cases, some filtering of this signal must be performed. This is the purpose of the state observer developed below.

V. DESIGN OF AN OBSERVER FOR THE VELOCITY FROM FREQUENCY MEASUREMENT

A. System dynamics and output map

A measurement of the velocity v has been defined earlier in Eq.(4). To filter it, we will design a state observer, relying on the dynamics below

$$\dot{v} = f_1(v,h,\theta) \triangleq \frac{-\rho_a(h) S \hat{C_D}(v,h) v^2}{2M} - g\sin(\theta)$$
$$y = f_2(v,h,p) \triangleq \frac{v}{2D}(P_1(v,h,p)^2 + P_2(v,h,p)^2)^{\frac{1}{4}} \cos\left[(\frac{1}{2}\arctan\left(\frac{P_2(v,h,p)}{P_1(v,h,p)}\right)\right]$$

Two of the variables appearing in the right-hand sides above are in fact known in advance, at least to a certain degree of accuracy, provided that they are well synchronized[2]: the planned altitude $h(t)$ and slope angle of the trajectory $\theta(t)$, and the real spinning rate $p(t)$ are known. This allows us to rewrite the dynamics as a single-state time-varying nonlinear dynamics

[2]which is easily done by detecting gun fire from any of the embedded signal, e.g. any of the accelerometers

$$\dot{v}(t) \triangleq f(v,t) \tag{5}$$
$$y(t) \triangleq g(v,t) \tag{6}$$

Various plots of the mappings f and g are reported in Figure 6 and Figure 7.

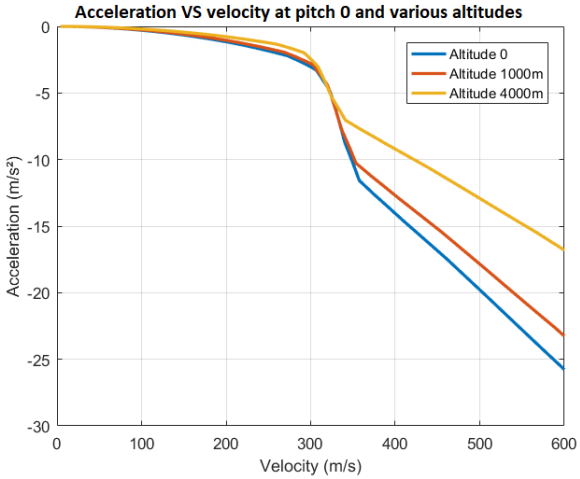

Fig. 6. Representation of $f(v,t)$ (for a fixed t, at various altitudes).

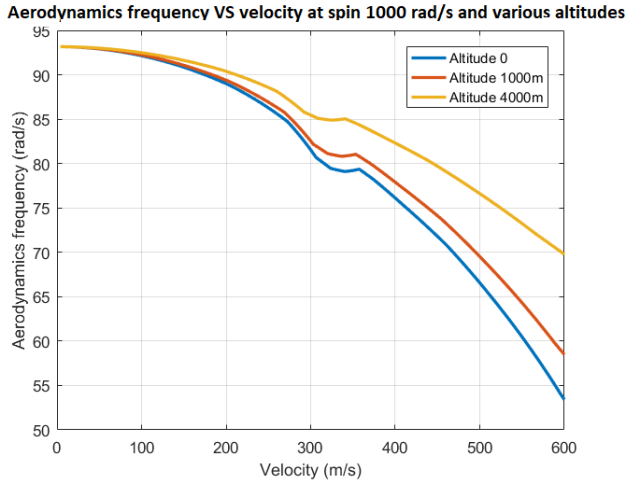

Fig. 7. Representation of $g(v,t)$ (for a fixed t, at various altitudes).

Observer design for this nonlinear dynamics(5)-(6) seems, at first, a routine problem. The main difficulty here is that g in (6) is not one-to-one. In fact, a general property stemming from the behavior of aerodynamic drag-induced effects near Mach 1.0 (see discussion in §III), is that for any given t, $v \mapsto \frac{\partial g}{\partial v}(v,t)$ *has, a fixed number N of zeros (at least 2)*, that we call $m_i(t)$ with

$$m_1(t) < ... < m_N(t)$$

To clarify, those zeros are linked to specific fixed Mach values. They represent time-varying critical velocities, because said velocities are linked to Mach values by the sound velocity at the altitude $h(t)$ reached at time t, via the corresponding air density.

This fact is illustrated in Figure 7, with $N = 2$ for a typical ballistic trajectory of a 155 mm shell. We may call this the *non-bijectivity of the frequency-velocity mapping in transonic regime*. Finally, one can also note that f becomes steep in the same regime (see Figure 6). However, it remains monotonic w.r.t. v at all times. Some (tedious) analytical study reveals that $\frac{\partial \hat{C}_D}{\partial v}$ remains small enough, for all v and t of interest in this study, so that $\frac{\partial f}{\partial v}$ stays strictly negative and bounded[3].

For a given trajectory, traveling through the atmosphere, the m_i are time-varying because the extremum points depends on the Mach number, and thus on the air density in addition to the velocity. For the rest of the analysis, we consider that the m_i are continuous and differentiable functions of the time (*de facto*, they are continuous and differentiable functions of the air density and the spinning rate, which vary continuously over time), without any further assumption on the aerodynamic coefficients.

For all applications considered in this article, i.e. shells, speed and time ranges, the mapping f is a contraction in the sense of [48], [49] as

$$\frac{\partial f}{\partial v} < -\gamma < 0$$

for some $\gamma > 0$.

B. Observer design

The observer is quite easy to design, using the fact that f defines a contractive mapping. However, the exponential convergence stemming from this property is not sufficient for practical application of velocity estimation (note that the total flight time is short). To speed-up the convergence, we make an active usage of the measurement y.

As discussed earlier, the output mapping is not one-to-one. Locally, it is monotonic, but since the estimate from the observer is the only way to guess whether the mapping is currently increasing or decreasing, there is no straightforward condition to determine the sign of the observer gain. This problem is relatively frequent in control system theory, see e.g. [50] and references therein.

What we propose is a gain-switching observer, following a classic approach [51], [52], where the gain is a function of the current estimate. To guarantee exponential convergence, we consider the squared error as candidate Lyapunov function and design the gain so that it is always decreasing. This is achieved by shutting-down the gain in certain areas near specific Mach numbers, where the derivative of g w.r.t. the velocity changes sign. The on-off times are tailored according to the properties of the aerodynamics model (upper and lower Lipschitz constants).

C. Main result : convergence of the velocity observer

Let k and ϵ be two strictly positive numbers. Consider the gain

$$K(\hat{v},t) \triangleq \chi(\hat{v},t) k \frac{\partial g}{\partial v}(\hat{v},t) \tag{7}$$

with

$$\chi(v,t) = \begin{cases} 0 \text{ if } v \in \bigcup_{i=1}^{N}]m_i(t) - \epsilon, m_i(t) + \epsilon[\\ 1 \text{ otherwise} \end{cases} \tag{8}$$

[3]Establishing this could be more involved for other shells, e.g. reentry vehicles for which trajectories cover much wider velocity and time ranges.

Then, one can state the following result:

Theorem 1 (Main result): Consider the state dynamics (5). Let us assume that there exists $M > 0$ such that $|v(0) - \hat{v}(0)| < M$, and that $\hat{v}(0) > m_N(0)$ and $v(0) > m_N(0)$. Then, there exists ϵ and k_M such that the observer $\hat{v}$ defined by $\dot{\hat{v}} = f(\hat{v},t) + K(\hat{v},t)(y - g(\hat{v},t))$ and (7)-(8) produces an estimation error $|v - \hat{v}|$ which converges exponentially to 0.

Proof:

Let δ and ϵ be two strictly positive numbers such that $\hat{v}(0) > m_N(0) + \epsilon$ and $v(0) > m_N(0) + \epsilon + \delta$ and $k_M > 0$ satisfies

$$k_M > \frac{1}{\alpha} \frac{m}{\ell} \tag{9}$$

and

$$k_M > \frac{-1}{\beta^2 T} \log\left(\frac{\epsilon}{M}\right) \tag{10}$$

where the following constants are defined (they depend solely on the trajectory under consideration)

$$T \triangleq \inf\{t \geq 0, v(t) \leq m_N(t) + \epsilon + \delta\}$$

$$m \triangleq \max\{\dot{m_N}(t), t \in [0,T]\} + \max\{-f(m_N(t) + \epsilon, t), t \in [0,T]\}$$

$$\ell \triangleq \min\{|g(m_N(t) + \epsilon + \delta) - g(m_N(t) + \epsilon, t)|, t \in [0,T]\}$$

$$\alpha \triangleq \min_{0 \leq t \leq T, m_N(t) + \epsilon \leq v \leq +\infty} (|\frac{\partial g}{\partial v}(v,t)|)$$

$$\beta \triangleq \max_{0 \leq t \leq T, m_N(t) + \epsilon \leq v \leq +\infty} (|\frac{\partial g}{\partial v}(v,t)|)$$

Note that α and β are properly defined as long as we prolongate our mapping of the aerodynamic coefficients by a continuous and differentiable saturation to the end of our mapping ; in practical, v stays bounded in a finite-flight (the shell has finite energy and the altitude has to remain positive), and $\hat{v}$, even though having a different dynamics, only gets closer to v as t increases, bounding him as well.

Set $V = \frac{1}{2}(v - \hat{v})^2$ as a candidate Lyapunov function ; it is strictly positive, and we will show its time derivative is strictly negative along the system trajectory for any initial conditions satisfying the assumptions of the statement. We will actually show the convergence to be exponential by ensuring $\dot{V} < -2\gamma V$.

By the mean-value theorem applied to f and g, separately, for any $t \geq 0$, there exists a_t and b_t in between v and $\hat{v}$ such that :

$$\dot{V} = (v - \hat{v})^2 (\frac{\partial f}{\partial v}(a_t,t) - K(\hat{v},t) \frac{\partial g}{\partial v}(b_t,t))$$

which expands as

$$\dot{V} = 2V \left(\frac{\partial f}{\partial v}(a_t,t) - \chi(\hat{v},t) k_M \frac{\partial g}{\partial v}(\hat{v},t) \frac{\partial g}{\partial v}(b_t,t) \right)$$

As we know it, $\frac{\partial f}{\partial v} < -\gamma < 0$. On the other hand the sign of the second factor is less obvious. In fact, from the definition of the indicator function (8), if $\chi(\hat{v},t)$ is non-zero, then $\frac{\partial g}{\partial v}(\hat{v},t)$ and $\frac{\partial g}{\partial v}(b_t,t)$ are of the same sign for any b_t in between v and $\hat{v}$. We will show firsthand that this is the case for $t \in [0,T]$, implying that $\dot{V} < -2\gamma V$

on that domain, then we will show that this inequality also holds for $t \geq T$ for a similar reason.

1) Before time T: By definition, for $t \in [0,T]$, $v(t) \geq m_N(t)+\epsilon+\delta$. Let us show that for $t \in [0,T]$, $\hat{v} \geq m_N(t)+\epsilon$.

Given any $t \in [0,T]$ such that $\hat{v}(t) = m_N(t) + \epsilon$, then $\dot{\hat{v}}(t) = f(m_N(t)+\epsilon,t) + k_M \frac{\partial g}{\partial v}(m_N(t)+\epsilon,t)(g(v,t) - g(m_N(t)+\epsilon,t))$.

We show, from (9), that in this case $\dot{\hat{v}}(t) > \dot{m_N}(t)$. This quite easily leads to the fact that for $t \in [0,T]$, $\hat{v} \geq m_N(t)+\epsilon$.

We thus concludes that for $t \in [0,T]$, $\chi(\hat{v},t) = 1$, and that $k_M \frac{\partial g}{\partial v}(\hat{v},t)\frac{\partial g}{\partial v}(b_t,t) < 0$.

As a result, $\dot{V} < -2\gamma V$ on $[0,T]$.

2) After time T: Let us show that $\dot{V}$ remains strictly less than $-2\gamma V$ after time T.

Because of (10), one gets $k_M > \frac{-1}{\beta^2 T} \log\left(\frac{\epsilon}{|v(0)-\hat{v}(0)|}\right)$ and obviously $\dot{V} < -2\beta^2 k_M V$ on $[0,T]$ by definition of β, we get $V(T) < V(0)e^{-2\beta^2 k_M T} < V(0)\left(\frac{\epsilon}{|v(0)-\hat{v}(0)|}\right)^2$ which gives us $|v(T)-\hat{v}(T)| < \epsilon$.

Let us assume that there exists a minimal $t_c > T$ where $\dot{V} \geq -2\gamma V$. For $t \in [T,t_c[$, we have $\dot{V} < -2\gamma V$ and thus $|v(t_c)-\hat{v}(t_c)| < \epsilon$.

As a result, there are two (exclusive) alternatives : either $\hat{v}(t_c)$ belongs to $\bigcup_{i=1}^{N}]m_i(t)-\epsilon, m_i(t)+\epsilon[$, which nullifies χ and sets the gain to zero ; or $\hat{v}(t_c)$ does not, and then obviously $\frac{\partial g}{\partial v}(v,t)$ is of the same sign as $\frac{\partial g}{\partial v}(\hat{v},t)$, because $|v(t_c)-\hat{v}(t_c)| < \epsilon$ and then neither of the $m_i(t_c)$ can be between $v(t_c)$ and $\hat{v}(t_c)$; in that case $k\frac{\partial g}{\partial v}(\hat{v},t)\frac{\partial g}{\partial v}(b_t,t) < 0$. Either way, $\dot{V}(t_c) < 2\gamma V$, which is a contradiction.

In summary, V is a Lyapunov function for our observation system $(v,\hat{v})$. The convergence is exponential, as $\dot{V} < -2\gamma V$ with $\gamma > 0$. This concludes the proof. ■

VI. EXPERIMENTAL RESULTS

The observer proposed in this article has been tested on real flight data, and, if the initialization is inaccurate, it represents a significant improvement compared to an open-loop estimation. Typical results obtained on experimental data are reported in Figure 8. The shell under consideration is a 155 mm in ballistic flight. An accurate measurement of its air velocity is obtained by a state-of-the-art ground radar. As is visible in Figure 8, our method allows one to approach this true value, even from a very poor initial estimate of the shell velocity (20% error). The flight last approx. 55 s. Transonic regime is reached at approx 9 s. The observer is able to improve its estimate up to approx. 30 s. when the shell reaches its culmination point (highest altitude). After this point, the yawing and pitching motions have too small magnitude to provide further information on the velocity. The estimate does not make much further progress past this point.

Several issues remained to be solved, as MUSIC algorithm only reads p, $p-\omega_n$ and $p-\omega_p$ during the ascending part of the flight, and p, $p-\omega_p$ after the peak ; as the accuracy on ω_p is really poor, we are able to construct the measurement ω_{meas} and run our observer during the ascending part of the flight only.

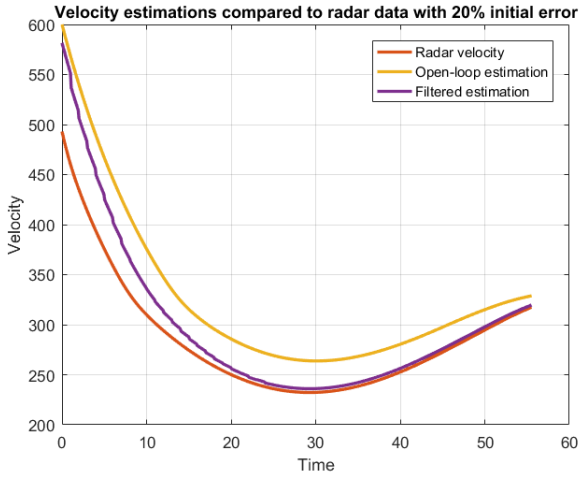

Fig. 8. Velocity Observer compared to an open-loop estimation (experimental results).

VII. CONCLUSIONS AND FUTURE WORKS

As we have illustrated it in last section, the estimation methodology has been tested on real flight data, and represents a significant improvement compared to an open-loop estimation.

Even though it is not the focus of this paper, one should remember we are considering here shells without thrust, controlled by impulsive actions near the end of the flight . The converging time of our observer thus is not relevant in that regard, as long as it has converged before the controller is used.

This estimation of the velocity enables us to use the aerodynamic model of the shell to carry out an incidence estimation, which is a prerequisite to know the orientation of the shell and integrating its position, and makes this a key part of any navigation algorithm. This is certainly a path to explore in future works.

As briefly told in the introduction, estimating the velocity is required to make full use of the aerodynamic model of the shell ; but the frequency analysis holds more information, as soon as one is able to measure the precession and nutation amplitudes as well. In fact, if the firing velocity is initialized correctly, the open-loop estimation of the velocity is already quite accurate ; using this estimation and the best-known aerodynamic coefficients (namely, the Drag and the Lift coefficient), one might be able, through a complete frequency analysis, to estimate the incidence of the shell without prior knowledge on the Magnus moment, overturning moment and pitch-damping moment coefficient.

Fig. 9. Toward a reduced aerodynamic model through low frequency analysis

REFERENCES

[1] M. D. Shuster, "Approximate algorithms for fast optimal attitude computation," *Proceedings of the AIAA Guidance and Control Conference*, pp. 88–95, 1978.

[2] I. Y. Bar-Itzhack, "REQUEST - a new recursive algorithm for attitude determination," *Proceedings of the National Technical Meeting of The Institude of Navigation*, pp. 699–706, 1996.

[3] D. Titterton and J. Weston, *Strapdown Inertial Navigation Technology*, 2nd ed. Reston, USA: The American Institute of Aeronautics and Aeronautics, 2004.

[4] J. L. Crassidis, F. L. Markley, and Y. Cheng, "Survey of nonlinear attitude estimation methods," *Journal of Guidance, Control and Dynamics*, 2007.

[5] P. Zarchan, *Tactical and Strategic Missile Guidance*. The American Institute of Aeronautics and Astronautics, 2007.

[6] D. Choukroun, "Novel methods for attitude determination using vector observations," Ph.D. dissertation, Technion, 2003.

[7] T. Hamel and R. Mahony, "Attitude estimation on SO[3] based on direct inertial measurements," in *Proceedings 2006 IEEE International Conference on Robotics and Automation, 2006. ICRA 2006.*, May 2006, pp. 2170–2175.

[8] J. L. Crassidis, F. L. Markley, and Y. Cheng, "Survey of nonlinear attitude estimation methods," *Journal of Guidance, Control, and Dynamics*, vol. 30, no. 1, pp. 12–28, 2007.

[9] A. Tayebi, S. McGilvray, A. Roberts, and M. Moallem, "Attitude estimation and stabilization of a rigid body using low-cost sensors," in *Decision and Control, 2007 46th IEEE Conference on*. IEEE, 2007, pp. 6424–6429.

[10] S. Berkane, A. Abdessameud, and A. Tayebi, "A globally exponentially stable hybrid attitude and gyro-bias observer," in *Decision and Control (CDC), 2016 IEEE 55th Conference on*. IEEE, 2016, pp. 308–313.

[11] R. Mahony, T. Hamel, and J.-M. Pflimlin, "Complementary filter design on the special orthogonal group SO(3)," in *Proc. of the 44th IEEE Conf. on Decision and Control, and the European Control Conference 2005*, 2005.

[12] ——, "Nonlinear complementary filters on the special orthogonal group," *IEEE Transactions on Automatic Control*, vol. 53, no. 5, pp. 1203–1218, June 2008.

[13] H. Fourati and D. E. C. Belkhiat, *Multisensor Attitude Estimation: Fundamental Concepts and Applications*. CRC Press, 2016.

[14] N. Metni, J.-M. Pflimlin, T. Hamel, and P. Souères, "Attitude and gyro bias estimation for a VTOL UAV," *Control Engineering Practice*, vol. 14, no. 12, pp. 1511 – 1520, 2006.

[15] D. Jung and P. Tsiotras, "Inertial attitude and position reference system development for a small UAV," in *AIAA Infotech at Aerospace*, 2007.

[16] M. D. Hua, G. Ducard, T. Hamel, R. Mahony, and K. Rudin, "Implementation of a nonlinear attitude estimator for aerial robotic vehicles," *IEEE Transactions on Control Systems Technology*, vol. 22, no. 1, pp. 201–213, 2014.

[17] I. Skog and P. Handel, "In-car positioning and navigation technologies – a survey," *IEEE Transactions on Intelligent Transportation Systems*, vol. 10, no. 1, pp. 4–21, 2009.

[18] B. O. Sunde, "Sensor modelling and attitude determination for micro-satellites," Master's thesis, NTNU, 2005.

[19] L. Magnis and N. Petit, "Rotation estimation for a satellite from sun sensors," in *Control Conference (ECC), 2013 European*. IEEE, 2013, pp. 852–859.

[20] J. C. Springmann, A. J. Sloboda, A. T. Klesh, M. W. Bennett, and J. W. Cutler, "The attitude determination system of the rax satellite," *Acta Astronautica*, vol. 75, pp. 120–135, 2012.

[21] J. K. Bekkeng and M. Psiaki, "Attitude estimation for sounding rockets using microelectromechanical system gyros," *Journal of Guidance, Control, and Dynamics*, vol. 31, no. 3, pp. 533–542, 2008.

[22] H. Lee, Y.-H. Choi, H.-C. Bang, and J.-O. Park, "Kalman filtering for spacecraft attitude estimation by low-cost sensors," *KSAS International Journal*, vol. 9, no. 1, pp. 147–161, 2008.

[23] J. C. Springmann and J. W. Cutler, "Optimization of directional sensor orientation with application to photodiodes for spacecraft attitude determination," *Journal of Guidance, Control, and Dynamics*, vol. 37, pp. 828–837, 2014.

[24] ——, "Flight results of a low-cost attitude determination system," *Acta Astronautica*, vol. 99, pp. 201–214, 2014.

[25] L. D. Fairfax and F. E. Fresconi, "Position estimation for projectiles using low-cost sensors and flight dynamics," *Journal of Aerospace Engineering*, vol. 27, no. 3, pp. 611–620, 2012.

[26] J. Rogers, M. Costello, T. Harkins, and M. Hamaoui, "Effective use of magnetometer feedback for smart projectile applications," *Navigation*, vol. 58, no. 3, pp. 203–219, 2011.

[27] Z. Zhao, G. Wen, X. Zhang, and D. Li, "Model-based estimation for pose, velocity of projectile from stereo linear array image," *Measurement Science Review*, vol. 12, no. 3, pp. 104–110, 2012.

[28] R. L. McCoy, *Modern exterior ballistics*, 2nd ed. Schiffer, 1998.

[29] J. Yu, X. Bu, C. Xiang, and B. Yang, "Spinning projectile's attitude measurement using intersection ratio of magnetic sensors," *Proceedings of the Institution of Mechanical Engineers, Part G: Journal of Aerospace Engineering*, 2016.

[30] S. Changey, E. Pecheur, and T. Brunner, "Attitude estimation of a projectile using magnetometers and accelerometers, experimental validation," in *Position, Location and Navigation Symposium - PLANS 2014, 2014 IEEE/ION*, 2014, pp. 1168–1173.

[31] S. Podjawerschek, E. Spahn, J. Horn, M. Brodmann, and R. Himmelsbach, "Distance and velocity estimation of projectiles based on doppler radar signals using a nonlinear discrete-time observer," in *Signal and Data Processing of Small Targets 2010*, vol. 7698. International Society for Optics and Photonics, 2010, p. 76980G.

[32] R. Vítek, "Influence of camera calibration technique on projectile velocity estimation," in *Military Technologies (ICMT), 2017 International Conference on*. IEEE, 2017, pp. 78–86.

[33] T. Recchia, W. Toledo, J. Cahayla, and E. Scheper, "Onboard sensor suite for determining projectile velocity," Apr. 30 2013, US Patent 8,433,460.

[34] C. Fernandez-Granda, G. Tang, X. Wang, and L. Zheng, "Demixing sines and spikes : Robust spectral super-resolution in the presence of outliers," *Information and Inference*, sep 2017.

[35] A. Fiot, S. Changey, C. Combettes, and N. Petit., "Estimation of air velocity for a high velocity spinning projectile using transerse accelerometers," in *2018 AIAA Guidance, Navigation, and Control Conference, AIAA SciTech Forum*, 2018.

[36] L. Landau and E. Lifchitz, *Mechanics*, 4th ed. MIR Moscou, 1982.

[37] R. D. Lorenz, *Spinning Flight*. Springer, 2006.

[38] S. Weiss, K.-F. Doherr, and H. Schilling, "Analytical solution and parameter estimation of projectile dynamics," *Journal of spacecraft and rockets*, vol. 32, no. 1, pp. 67–74, 1995.

[39] A. Carrière and L.-R. Oudin, "Applications du calcul formel à la balistique," *Theoretical Computer Science*, vol. 187, no. 1, pp. 263 – 284, 1997.

[40] M. Costello and T. Jitpraphai, "Determining angular velocity and angular acceleration of projectiles using triaxial acceleration measurements," *Journal of spacecraft and rockets*, vol. 39, no. 1, pp. 73–80, 2002.

[41] L. Magnis and N. Petit, "Angular velocity nonlinear observer from single vector measurements," *Automatic Control, IEEE Transactions on*, vol. 61, no. 9, pp. 2473–2483, 2016.

[42] J. Shang, Z. Deng, M. Fu, and S. Wang, "A high-spin rate measurement method for projectiles using a magnetoresistive sensor based on time-frequency domain analysis," *Sensors*, vol. 16, no. 6, p. 894, 2016.

[43] L. Magnis and N. Petit, "Angular velocity nonlinear observer from vector measurements," *Automatica*, vol. 75, pp. 46–53, 2017.

[44] P. Cardou and J. Angeles, "Estimating the angular velocity of a rigid body moving in the plane from tangential and centripetal acceleration measurements," *Multibody System Dynamics*, vol. 19, no. 4, pp. 383–406, 2008.

[45] S. Mallat, *A wavelet tour of signal processing: the sparse way*. Academic Press, 2008.

[46] M. H. Hayes, *Statistical Digital Signal Processing and Modeling*. John Wiley & Sons, 1996.

[47] C. Fernandez-Granda and E. J. Candès, "Towards a mathematical theory of super-resolution," *Communications on Pure and Applied Mathematics*, vol. 67, no. 6, pp. 906–956, 2014.

[48] N. N. Krasovskii, *Problems of the theory of Stability of Motion*. MIR, translated by Stanford University Press, 1963.

[49] W. Lohmiller and J.-J. E. Slotine, "On contraction analysis for nonlinear systems," *Automatica*, vol. 34, no. 6, pp. 683 – 696, 1998.

[50] D. Carnevale, D. Karagiannis, and A. Astolfi, "Reduced-order observer design for systems with non-monotonic nonlinearities," in *Decision and Control, 2006 45th IEEE Conference on*. IEEE, 2006, pp. 5269–5274.

[51] A. Alessandri and P. Coletta, "Switching observers for continuous-time and discrete-time linear systems," in *American Control Conference, 2001. Proceedings of the 2001*, vol. 3. IEEE, 2001, pp. 2516–2521.

[52] A. A. Chunodkar and M. R. Akella, "Switching angular velocity observer for rigid-body attitude stabilization and tracking control," *Journal of Guidance, Control, and Dynamics*, vol. 37, no. 3, pp. 869–878, 2014.